CVI
Journals.ASM.org

Immunologic Characterization of a Rhesus Macaque H1N1 Challenge Model for Candidate Influenza Virus Vaccine Assessment

Jason A. Skinner,[a] Sandra M. Zurawski,[a] Chie Sugimoto,[b] Heather Vinet-Oliphant,[b] Parvathi Vinod,[a] Yaming Xue,[a] Kasi Russell-Lodrigue,[b] Randy A. Albrecht,[c] Adolfo García-Sastre,[c] Andres M. Salazar,[d] Chad J. Roy,[b] Marcelo J. Kuroda,[b] SangKon Oh,[a] Gerard Zurawski[a]

Baylor Institute for Immunology Research, Dallas, Texas, USA[a]; Tulane National Primate Research Center, Covington, Louisiana, USA[b]; Icahn School of Medicine at Mount Sinai, New York, New York, USA[c]; Oncovir, Inc., Washington, DC, USA[d]

Despite the availability of annually formulated vaccines, influenza virus infection remains a worldwide public health burden. Therefore, it is important to develop preclinical challenge models that enable the evaluation of vaccine candidates while elucidating mechanisms of protection. Here, we report that naive rhesus macaques challenged with 2009 pandemic H1N1 (pH1N1) influenza virus do not develop observable clinical symptoms of disease but develop a subclinical biphasic fever on days 1 and 5 to 6 postchallenge. Whole blood microarray analysis further revealed that interferon activity was associated with fever. We then tested whether type I interferon activity in the blood is a correlate of vaccine efficacy. The animals immunized with candidate vaccines carrying hemagglutinin (HA) or nucleoprotein (NP) exhibited significantly reduced interferon activity on days 5 to 6 postchallenge. Supported by cellular and serological data, we conclude that blood interferon activity is a prominent marker that provides a convenient metric of influenza virus vaccine efficacy in the subclinical rhesus macaque model.

Respiratory tract infections caused by influenza viruses are estimated to result in 3 to 5 million clinical infections and 250,000 to 500,000 fatalities per year (http://www.who.int/mediacentre/factsheets/fs211/en/). Prior to 2009, influenza A viruses of the H1N1 and H3N2 subtypes and influenza B viruses were mainly responsible for seasonal disease outbreaks. Since the emergence of pandemic H1N1 (pH1N1) influenza virus in 2009, this swine-origin influenza A virus has supplanted the previous seasonal H1N1 strain (1).

Both humoral and cellular responses are important for immunity against influenza virus infection. The surface hemagglutinin (HA) protein is one of the primary targets for antibody-mediated viral neutralization (2). This selective pressure drives HA diversity and limits the cross-reactivities of HA-specific antibodies. HA-specific IgG antibodies lining the respiratory tract can protect against reinfection (3). Cellular immune responses are generated against both surface and internal viral proteins, including the highly conserved nucleoprotein (NP). These antigen-specific responses are capable of targeting infected cells for lysis by cytotoxic T cells (CTLs). After infection, memory CTLs reside in both the lungs and lymphoid organs, where they are poised to respond to subsequent influenza virus infections (4). Despite being directed to an internal viral protein, NP-specific antibodies may also contribute to protection (5); however, the mechanism by which this occurs is unknown.

In response to the antigenic shift observed in 2009, previously characterized nonhuman primate (NHP) models used to evaluate H3N2 and seasonal H1N1 virulence were reassessed using the pH1N1 virus (6–10). These studies revealed species-specific differences in the host responses between rhesus and cynomolgus macaques. Cynomolgus macaques infected with strain influenza A/California/04/2009 (H1N1) (pH1N1 Cal04) virus exhibited moderately severe clinical signs by day 6 postinfection, with a concurrent activation of the inflammatory response genes in the lung (11). In comparison, rhesus macaques infected with the same pH1N1 strain remained asymptomatic despite sustained viral shedding for 21 days postinfection (10). This subclinical response characterized by the absence of clinical signs following experimental infection has thus far limited the use of the rhesus macaque challenge models to assess candidate vaccine efficacy.

In this study, we assessed the capability of a naturally aspirated pH1N1 mixed-particle aerosol infection to increase the clinical signs of pH1N1 infection in rhesus macaques. In addition to the commonly used metrics of body temperature and viral titers, we employed whole blood mRNA microarray-based monitoring to increase sensitivity to systemic immunologic changes following challenge.

As a proof-of-concept, we first tested this strategy to examine the protection afforded by two candidate dendritic cell (DC)-targeting vaccines engineered to deliver HA and NP antigens to rhesus macaque antigen-presenting cells (APCs). In a pilot test, HA was linked to an anti-LOX-1 antibody vehicle, which was coadministered with anti-dendritic cell immunoreceptor (DCIR) antibody linked to NP, and both were adjuvanted with CpG. The anti-LOX-1 vaccine was selected based on previous studies that showed it evokes Th1-type responses (12) consistent with the development of protective antibody responses. The anti-DCIR-fusion protein delivering NP was shown to elicit antigen-specific CTL responses *in vitro* (13). The results of this pilot study were used to justify a larger follow-up study in which separate anti-

Received 11 August 2014 **Returned for modification** 29 August 2014
Accepted 1 October 2014
Published ahead of print 8 October 2014
Editor: H. F. Rosenberg
Address correspondence to Gerard Zurawski, gerardz@baylorhealth.edu.
Supplemental material for this article may be found at http://dx.doi.org/10.1128/CVI.00547-14.

doi:10.1128/CVI.00547-14

CD40-HA–poly(ICLC) and anti-CD40-NP–poly(ICLC) vaccine candidates were assessed via a microarray-based blood interferon signature, complemented with both serologic and cellular data, as a metric of protection from signs of infection.

MATERIALS AND METHODS

Animals. The studies were carried out in 24 approximately 4- to 7-year-old (male and female) rhesus macaques (*Macaca mulatta*). The macaques were examined daily for evidence of clinical illness, including decreased appetite, dehydration, increased respiratory rate, and increased respiratory effort. All animal experiments were conducted at the Tulane National Primate Research Center (TNPRC) in compliance with the guidelines of the animal care and use committees at the Baylor Research Institute and the TNPRC.

Animal infections. The animals were exposed to pH1N1 (Cal04) influenza virus using conventional methodology that was previously established for infectious mixed-particle aerosol challenge in nonhuman primate species (14). Inductive plethysmography, which measures the volume of air breathed per minute by each individual animal, was performed just before the exposure. Briefly, the animals were placed in a class III biological safety cabinet with only the head in the exposure chamber. Influenza virus at the appropriate concentration for each animal based on the plethysmography data for each animal obtained 2 days before the exposure was used to better estimate the target inhaled dose. The aerosols were generated directly in the head-only chamber using a Collison three-jet nebulizer (BGI, Inc.) with a fully automated management control system (Biaera, Inc.). The aerosol efficiency (effect of aerosolization upon artificially generated influenza aerosols) was determined prior to the animal exposures in order to estimate the actual delivered dose. The aerosol efficiency was calculated to be 10^{-9}. This translates into 1 PFU per 10^9 aerosolized viral particles. The aerosol size for these exposures was measured at ≈2-μm mass median aerodynamic diameter (MMAD). The aerosol samples were continuously obtained during the exposure, and the concentrations of these samples were determined by plaque assay. The aerosol concentrations were determined, and the inhaled dose for each animal was calculated by multiplying the empirically determined aerosol exposure concentration (PFU/liter of air) in the chamber by the volume of air estimated to have been breathed by the animal. The final dose delivered in the form of a small-particle aerosol was expressed as PFU/animal. Immediately after exposure to small-particle aerosols of influenza, the animal was removed from the exposure apparatus and again placed in dorsal recumbency. Thereafter, a custom long-tip MicroSprayer aerosolizer (Penn-Century, Inc.) that was fitted with a high-pressure syringe was placed proximal to the carina. It was visualized with a laryngoscope to confirm proper placement, and 1 ml of the appropriate viral strain was administered into the left and right main bronchi. The aerosol particles generated during this portion of the exposure were measured at an MMAD of ≈10 μm (data not shown) and constituted large-particle aerosol exposure relative to the size distribution represented in the exposure modality preceding this procedure. The final influenza virus dose used was cumulative and comprised the two modalities (small- and large-particle exposure) in the animal infections. The group mean ± standard deviation (SD) dose (for small-particle exposure) was $1.0 \times 10^6 \pm 1.5 \times 10^6$ PFU/animal. Due to the aerosol efficiency of 10^{-9}, approximately 1×10^{15} aerosol-inactivated virus particles accompanied the live dose into each animal. The large-particle dose was 2.2×10^7 PFU/animal, which approximates a cumulative dose (small- plus large-particle exposures) of 2.3×10^7 PFU/animal plus the 1×10^{15} aerosol-inactivated viral particles.

The animals that received the UV-inactivated virus received the same total dose of viral particles as described above (2.3×10^7 UV-inactivated viral particles plus 1×10^{15} aerosol-inactivated virus particles). Physical examinations were regularly performed on the animals following infection. Manually obtained temperature, heart rate, and respiratory rate data were recorded for verification with the telemetry data. Thoracic auscultation was performed to assess the changes in lung function; none were noted. Swabs of the pharynx and upper airway were collected for viral analysis to determine shedding.

Telemetry. Subcutaneous radio telemetry transmitters combined with sensors capable of detecting biopotential signals of an electrocardiogram (ECG), as well as thermistor-type sensors capable of detecting temperature signals (T31F-8b; Königsberg Instruments [KI], Inc.), were surgically implanted in eight rhesus macaques under aseptic conditions. Following surgical implantation, the animals were housed in rooms and cages specifically designed with cage-mounted antennas (TR38-1FG; Königsberg Instruments, Inc.) that were configured to receive and transmit signals to a KI data acquisition base station. The data collection was continuous and recorded for periods of 24 to 48 h using the CA recorder (Data Integrated Scientific Systems [DISS], Dexter, MI). The data parameters and analysis results recorded over the course of the study included (i) ECG Online (EOL), in which ECG signal amplitudes and various intervals were measured and recorded for heart rate (data not shown), and (ii) a mean analysis for body temperature measurements.

The telemetric parameters, including heart rate and core body temperature, were reported as hourly averages (data average interval) for 1-h observation intervals, with each animal serving as its own control. Baseline preexposure data averages for all animals were generated from each respective control subject for a minimum of 1 week. The preexposure data were aligned by the time of day over a 24-h period and averaged to establish baseline detection thresholds. The individual postexposure data were aligned by time and compared against the preexposure values for each animal. A fever hour was defined as any hourly measurement that was >1.5 times the maximum standard deviation of the control averages.

Vaccines. The dendritic cell (DC)-targeting vaccines used in this study were chimeric mouse variable region-human IgG4 constant region antibodies fused to influenza virus antigens via the H-chain C-terminal anti-human LOX-1 15C4-HA1s (GenBank accession no. KM246787) with nucleotides encoding a proximal SpeI site preceding (AAT79550.1) residues 651 to 667, with a T-to-N change at position 672 and a distal NheI site inserted into the C-terminal NheI site, followed by influenza A virus [A/California/04/2009 (H1N1)] hemagglutinin (HA) (FJ966082.1) residues 1129 to 2073 preceding six C-terminal His residues. This is coexpressed with an anti-LOX-1 15C4 chimeric light chain (GenBank accession no. KM246788). The 15C4 antibody binds efficiently to recombinant rhesus macaque LOX-1 ectodomain protein (S. M. Zurawski, unpublished data) and binds to $CD11c^+$ and $CD14^+$ cells in the peripheral blood mononuclear cells (PBMCs) of cynomolgus macaques (12, 15). Anti-human DCIR 9E8-NP (GenBank accession no. JX002667) with influenza A virus [A/environment/Viet Nam/1203/2004 (H5N1)] segment 5 nucleocapsid protein (NP) (GU052421.1) bases 1419 to 2913 with six C-terminal His codons inserted at the H chain C-terminal NheI site was also used. This is coexpressed with an anti-DCIR 9E8 light chimeric chain (GenBank accession no. JX002666). The 9E8 antibody binds efficiently to recombinant rhesus macaque DCIR ectodomain protein (S. M. Zurawski, unpublished data) and binds to various antigen-presenting cell types of cynomolgus macaques (15). Anti-human CD40 12E12-HA1s (GenBank accession no. HQ738666.1) is configured like the anti-human LOX-1 15C4-HA1s described above. It is coexpressed with an anti-CD40 12E12 chimeric light chain (GenBank accession no. HQ738667.1). The 12E12 antibody binds efficiently to recombinant CD40 ectodomain from rhesus macaques and to DCs from cynomolgus macaques (15). A previous study showed that the dimeric HA1 domain expressed as a C-terminal H-chain antibody fusion can fully deplete protective anti-HA1 antibodies and can generate protective immune responses in mice (16). Anti-human CD40 12E12-NP (GenBank accession no. HQ738666.1) is configured like anti-human DCIR 9E8-NP. They were coexpressed with their cognate chimeric light chain partners. Vectors, procedures for deriving stably transfected CHO-S cells, and the production, purification, formulation, and quality assurance of the recombinant DC-targeting vaccines were as described previously (16, 17).

Immunizations. For the pilot study, 100 μg of each targeting vaccine, anti-LOX-1-HA and anti-DCIR-NP, were coadministered with 1 mg of CpG on the dorsa of the animals between the shoulder blades by intradermal injection at five sites with 0.2 ml of vaccination material at each site. Boosts matching the initial vaccination were conducted at 6 and 12 weeks after priming. The CpG oligonucleotide 1018 ISS (provided by Dynavax Technologies) was selected based on known safety and ability to stimulate DC maturation and B-cell activation (18). The hemagglutinin inhibition (HAI) assay titers in these three animals were 40, 80, and 40 two weeks after both the 1st and 2nd boost and were 20, 40, and 40 four weeks after the 2nd boost. In the follow-up study, anti-CD40-HA–poly(ICLC), anti-CD40-NP–poly(ICLC), and medium–poly(ICLC) and influenza virus (Fluzone) immunizations were compared. Based on a recent study in mice showing efficacy protective antibody and T-cell responses (16), we targeted CD40. The CD40-targeting vaccines and medium controls were combined with poly(ICLC) (Hiltonol; Oncovir, Inc.) as an adjuvant based on its safety and immune activation properties (19). In total, 100 μg of vaccine and 1 mg of poly(ICLC) were coadministered on the dorsa of the animals between the shoulder blades by intradermal injection at five sites with 0.2 ml of vaccination material at each site. Full human-dose Fluzone vaccinations were given intramuscularly in the quadriceps muscle at each of the prime and boost vaccinations. Each animal was vaccinated three times, with 6 weeks between the immunizations. The injection sites were monitored for adverse localized reactions following each vaccination, and none were noted.

Cell preparation. The PBMCs were separated from EDTA anticoagulated whole blood using Ficoll density gradient centrifugation. The whole blood was centrifuged at 800 × *g* for 10 min at 20°C to collect plasma. After the removal of plasma, the blood cell fraction was resuspended in phosphate-buffered saline (PBS) and overlaid on Ficoll-Paque Plus (GE Healthcare). The samples were centrifuged at 400 × *g* for 30 min at 20°C. The mononuclear cell layer was collected and washed twice with 2% fetal calf serum (FCS)-PBS. The cells were counted and frozen at 1×10^7/ml/cryovial in Bambanker cell freezing medium (Lymphotec). The cells were stored at −80°C for 1 day and then stored in liquid nitrogen until shipping to the Baylor Institute for Immunology Research.

IFN-γ ELISPOT. Frozen PBMCs were thawed and washed in Advanced RPMI with 1× CTL wash medium (Cellular Technology Limited), 1% GlutaMAX (Gibco Life Technologies), 50 U/ml Benzonase (Emprove Bio), and 50 μg/ml Primocin (InvivoGen). The cells were resuspended at a concentration of 3.3×10^6/ml in CTL test medium (Cellular Technology Limited) supplemented with GlutaMAX and Primocin, as above. NHP gamma interferon (IFN-γ) enzyme-linked immunosorbent spot assay (ELISPOT) analysis was performed on ELISpot PRO monkey IFN-γ 3420M-2HPW-10 plates (Mabtech). The plates were prepared with 5× PBS wash, followed by blocking with 1% bovine serum albumin (BSA) in PBS (1 h at 37°C), washing 2× with PBS, and pretreatment in CTL test medium for 30 min at 37°C. The total volume per well was 150 μl, consisting of 2.5×10^6 cells in 75 μl added to 75 μl of medium containing control matrix, 2 μM peptide, or 10 μg/ml protein. Anti-CD3 was used as the polyclonal activation control, as per the manufacturer's instructions. The plates were incubated at 37°C in 7% CO_2 for 36 h and then developed according to the manufacturer's protocol. The plates were air-dried, shipped, and read by ZellNet Consulting. The group comparison statistics were calculated and plotted using GraphPad Prism 5 (GraphPad Software, Inc.).

Antigen-specific IgG titers. To determine the antigen (Ag)-specific antibody (Ab) titers, we used a modified Luminex bead-based assay that utilized a noncovalent assembly of antigen to beads using dockerin-cohesin interaction (16). The cellulose-binding domain from the *Clostridium acetobutylicum* CipA protein fused to dockerin (CBD-Doc) was conjugated to SeroMAP Luminex carboxylated beads at 25 μg per 5×10^6 beads, using the manufacturer's 2-step carboxylation protocol. Each CBD-Doc-coated bead set was incubated with individual cohesin antigen at a ratio of 10 μg/ml to 6.4×10^4/ml of beads in 1× PBS (Ca^{2+}/Mg^{2+}), 1% BSA, and 0.05% T20 (wash buffer) for a minimum of 2 h; they were then washed 3 times to remove any excess unbound antigen. Serum (or plasma) was prepared for incubation with this bead complex by completing a serial titration in wash buffer. The serial titration was initiated at 1:250 and carried over a 3- to 4-log range. To 50 μl of the titrated serum (plasma), 50 μl of the prepared complexed SeroMAP beads was added in 1.2-mm filter membrane 96-well microtiter plates (MABVN1250; Millipore Corp.) in a multiplex format. The incubation with beads and serum continued on a shaking platform overnight at 4°C. After three washes, 2 μg/ml of PhycoLink goat anti-human IgG (Fc-specific) R-phycoerythrin was added for an additional 1 h. The beads were washed twice, resuspended in 125 μl of wash buffer with 0.2% paraformaldehyde (PFA), and read on a Bio-Plex 200 (Bio-Rad). The mean fluorescent intensities were plotted versus the titration dilutions. The titers were defined as the inverse of the half-maximal effective concentration ($1/EC_{50}$). The antigens for this assay were prepared as follows. Cohesin-NP5 protein was prepared using an *Escherichia coli* expression plasmid encoding avian influenza NP [A/Viet Nam/1203/2004 (H5N1)] (ABC66760.1) residues 1 to 498 inserted distal to cohesin and proximal to six histidine residues. The parent vector and protein production of the soluble protein were as described in Flamar et al. (16), with the following exceptions: the cells were lysed in 50 mM morpholineethanesulfonic acid (MES) (pH 6.5), and the supernatant from 2 liters of cells was passed over a 20-ml HiPrep 16/10 Q XL column (Pharmacia) in the same buffer before the flowthrough was adjusted with buffer A of Ni^{2+} affinity chromatography. For coating the beads, CBD-Doc was also expressed in *E. coli* from a pET28 vector with the cellulose binding domain of the primary scaffoldin protein from *Clostridium thermocellum* (JX966414.1) residues 6049 to 6769 inserted into the NheI site of the vector; this was accomplished by converting the original NheI site to GCTAGT and then inserting the double dockerin domain of *C. thermocellum* CelD (X04584.1) residues 1924 to 2147 with TAA appended into the NheI-NotI interval. Cell growth, supernatant preparation, flowthrough Q Sepharose, and purification via Ni^{2+} affinity chromatography were as described previously (16). Cohesin-HA1 was expressed in *E. coli* from a pET28 vector with a gene sequence encoding the 7th cohesin domain of *C. thermocellum* CipA (AAG15504.1) residues 1 to 164, with R21N, E54E, and S109E changes. These changes were preceded by codons for serine and methionine inserted between the NdeI and NheI sites with influenza A virus A/California/04/2009 (H1N1) (FJ966082.1) residues 52 to 966 (HA1 domain) with appended CATCACCATCACCATCACTGA and then inserted between the NheI and NotI sites. Inclusion bodies were prepared, solubilized, refolded, and purified via Ni^{2+} affinity chromatography as described previously (16). The group comparison statistics were calculated and plotted using GraphPad Prism 5 (GraphPad Software, Inc.).

Influenza hemagglutinin inhibition assays. Hemagglutination inhibition (HAI) assays were conducted as described previously (20). Briefly, the A/California/07/09 influenza virus vaccine composition for the 2010-2011 influenza season were propagated in 8-day-old specific-pathogen-free embryonated hen eggs (Charles River). The HAI assays were performed as previously described for the detection of neutralizing antibodies (20). Briefly, 2-fold serial dilutions of monkey serum were mixed and preincubated in 96-well V-bottom microtiter plates for 30 min at room temperature with the indicated influenza virus vaccine strain. The HAI assays were developed by adding a 0.5% suspension of turkey red blood cells (Lampire Biological Laboratories) and incubating them until the red blood cells pelleted in the control wells containing saline only. The group comparisons and unpaired *t* tests were calculated and plotted using GraphPad Prism 5 (GraphPad Software, Inc.).

Microarray sample collection. One milliliter of macaque blood was drawn into Na-Li heparin blood collection tubes (BD Biosciences). Next, 500 μl of this blood was immediately aliquoted into freezer tubes containing 1.5 ml of Tempus reagent. All samples were thoroughly vortexed for 15 s to facilitate RNA stabilization. The samples were stored at −80°C until RNA extraction.

RNA isolation and microarray hybridization. Total RNA was isolated from the whole blood lysate using the MagMAX-96 blood RNA isolation kit (Applied Biosystems), according to the manufacturer's instructions. Following extraction, an Agilent 2100 Bioanalyzer (Agilent) was used to attain the RNA integrity numbers (RIN) for each sample. All samples with RIN values of >5.5 were retained for further processing. The RNA yields were attained using a NanoDrop 8000 (NanoDrop Technologies). Both the RIN and yield data were managed using a laboratory information management system (LIMS) for quality control and sample tracking.

After RNA extraction and quality control analysis, globin mRNA was depleted from a portion of each total RNA sample using the GLOBINclear-Human 96-well format kit (Ambion). This was then followed by another round of RIN and yield determinations for quality control purposes. All samples passing quality control were then amplified and labeled using the Illumina TotalPrep-96 RNA amplification kit (Ambion). The RNA input for this reaction was 250 ng. Next, 750 ng of the amplified labeled RNA was hybridized overnight to Illumina HT12 V4 BeadChips (Illumina). Following hybridization, each chip was washed, blocked, stained, and scanned on an Illumina BeadStation 500, according to the manufacturer's protocols.

Microarray normalization. The Illumina BeadStudio version 2 software was used to generate the signal intensity values from each scanned array, subtract background signal, and scale each microarray to the median average intensity for all samples.

Molecular distance to health. Molecular distance to health is a quantitative approach to cluster analysis results in the computation of a score representing the "molecular distance" of a given sample relative to a baseline (e.g., prechallenge controls). This analysis was performed by merging the transcripts contained within each cluster into a single gene list containing the raw expression data for each sample. The distance of each sample from the uninfected control baseline was calculated in four steps. (i) The first step was establishing the baseline. For each gene, the average expression level and standard deviation of the uninfected control group were calculated. (ii) Step 2 was calculating the distance of an individual gene from the baseline. The difference in the raw expression level from the baseline average of a gene was determined for a given sample. Next, the number of standard deviations from baseline represented by the difference in expression was calculated. (iii) Step 3 consisted of applying filters. Qualifying genes had to differ from the average baseline expression by ≥100 raw intensity units and 2 standard deviations. (iv) The last step was calculating a global distance from baseline. The numbers of the standard deviations for all qualifying genes were added to yield a single value, the global distance of the sample from the baseline.

Linear mixed-model analysis of longitudinal data. In the linear mixed-model analysis, the baseline transcriptional activities were determined for all macaques prior to challenge at day 0. For each macaque, the day −7 and 0 baseline samples were used and combined across treatment groups to create a shared baseline to which all postchallenge time point groups were compared. Statistical analyses of $\log_2$-transformed microarray data were performed using the SAS software (version 9.3) and JMP Genomics (version 6) (SAS Institute, Inc.). A linear mixed-model analysis (LMMA) accounting for repeated measures (repeated within each macaque) and unequal time point spacing was employed to test for significant differences in the gene expression between each postchallenge time point and the shared baseline. In the case of Fig. S2 in the supplemental material, the LMMA that was performed was a direct contrast between the vaccinated and unvaccinated groups at each time point and not to a shared baseline. A 0.05 false-discovery rate was employed for all hypothesis testing.

Nucleotide sequence accession numbers. The dendritic cell (DC)-targeting vaccines used in this study were chimeric mouse variable region-human IgG4 constant region antibodies fused to influenza virus antigens via the H-chain C-terminal anti-human LOX-1 15C4-HA1s, under GenBank accession no. KM246787, and an anti-LOX-1 15C4 chimeric light chain, under GenBank accession no. KM246788.

Microarray data accession number. The microarray data can be downloaded via the GEO Omnibus under accession no. GSE60009.

RESULTS

Characterization of clinical and lymphocyte responses to mixed-particle aerosol pH1N1 influenza challenge. Previous pH1N1 infections of rhesus macaques have relied on high-dose administration of virus to tracheal, nasal, ocular, and oral mucosal surfaces. This resulted in limited clinical signs despite the recovery of virus at multiple days postinfection (6, 11). In this study, we challenged naive animals with a mixed-particle aerosol composed of large and small virus particles. This mixed-particle aerosol approach was chosen to enhance the penetration of viral particles deep into the respiratory tract, with the goal of increasing the clinical signs of infection. This mixed-particle aerosol challenge to naive animals ($n = 3$) resulted in a biphasic increase in body temperature on days 1 and 6 postinfection (6.3 ± 3.8 h of fever duration on day 1 postinfection and 15.3 ± 4.5 h of fever duration on day 6 postchallenge (Fig. 1A; see also Fig. S1 in the supplemental material). Notably, after the resolution of fever on day 6 postinfection, there appeared to be a low-level residual fever up to 20 days postinfection in animals challenged with live virus but not in those challenged with the same dose of UV-inactivated virus. The close monitoring of animal behavior following challenge did not indicate any outward clinical malaise, suggesting that the intensity of the fever was insufficient to yield additional clinically observable signs.

Interestingly, the animals ($n = 2$) immunized in a pilot study with an experimental vaccine combining anti-LOX-1-HA and anti-DCIR-NP with CpG-B that was coadministered 8 months before showed a shorter duration of fever than that seen in naive animals (0.5 ± 0.7 versus 15.3 ± 4.5 h of fever, respectively, on day 6; $P = 0.02$, unpaired t test) (Fig. 1A).

The circulating IgG titers were determined for HA (Fig. 1B) and NP (Fig. 1C) both pre- and postchallenge for each of the three animal groups. The macaques challenged with 2.3×10^7 PFU-equivalent dose/animal of UV-inactivated virus failed to exhibit HA- or NP-specific antibody titers. Compared to the naive macaques, the previously vaccinated macaques had significantly higher baseline anti-HA antibody titers ($P = 0.04$, unpaired t test). The anti-NP titers in the vaccinated macaques trended higher at baseline but did not achieve significance over the titers measured in naive animals ($P > 0.05$, unpaired t test). Eight days postchallenge, both the anti-HA and anti-NP titers were boosted and were significantly higher in the previously vaccinated group than those in the naive animals ($P < 0.05$, unpaired t test). Only the anti-NP titers remained significantly higher in the vaccinated group than those in the naive animals 20 days postchallenge ($P = 0.002$, unpaired t test). The hemagglutination inhibition (HAI) assay titers were determined 7 days prior to challenge and then again on day 20 postchallenge (Fig. 1D). All macaques exhibited HAI assay titers below the accepted neutralization threshold of 40 at seven days before challenge. The two previously vaccinated animals did mount neutralizing HAI assay titers immediately following vaccination (see Materials and Methods); however, these titers waned by 8 weeks following the second boost (Fig. 1D). Only those animals challenged with live virus exhibited HAI assay titers of >40 at 20 days postchallenge. Similarly, IFN-γ-producing antigen-spe-

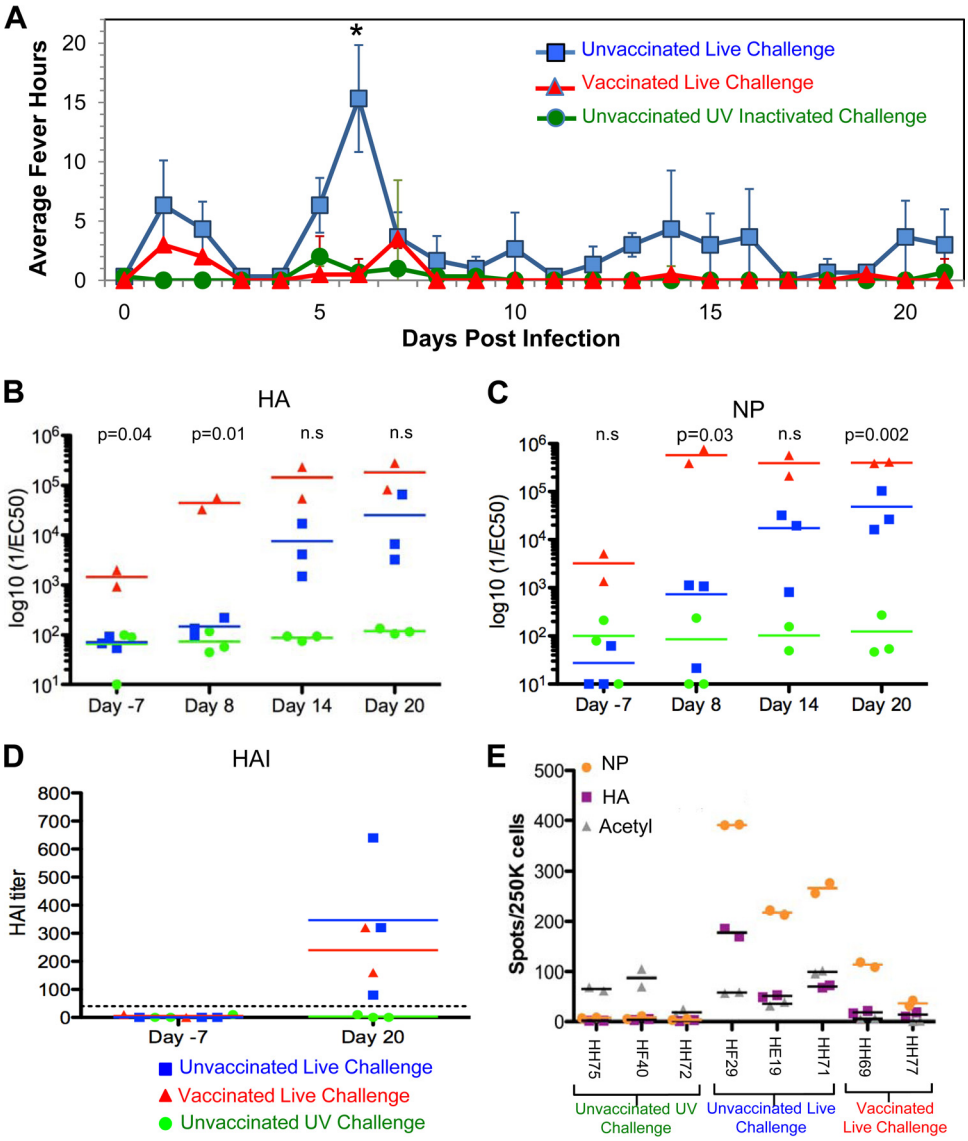

FIG 1 Previous vaccination elicits differential subclinical and cellular responses following live-virus challenge. (A) Physiological responses of vaccinated rhesus macaques to pH1N1 challenge. Fever hours (number of hours of fever) are displayed as daily mean ± SD for unvaccinated animals with live challenge (■), vaccinated animals with live challenge (▲), and unvaccinated animals with UV-inactivated challenge (●). Significant changes among the groups were compared statistically (unpaired *t* test.) Significant results ($P < 0.05$) are indicated on the plot. (B and C) Circulating HA and NP antibody titers were quantified by ELISA 7 days prior to pH1N1 challenge and on 8, 14, and 20 days postchallenge. The *P* values indicate the intraday comparison of previously vaccinated animals (anti-LOX-1-HA–anti-DCIR-NP5 with CpG) and unvaccinated animals receiving live pH1N1 challenge (unpaired *t* test). n.s., nonsignificant. The horizontal line represents the mean for each group. (D) HAI viral neutralization assay. The dotted line indicates the accepted HAI titer required for neutralization. (E) Day 20 IFN-γ-producing T cells responding to anti-LOX-1-HA1 and anti-DCIR-NP5 proteins were quantified using ELISPOT. Note that the pH1N1 restimulation peptide pool concentration was 0.02 μg/ml for the prevaccinated live-virus challenge group, while the unvaccinated UV-inactivated-virus challenge and unvaccinated live-virus challenge groups were stimulated at 0.1 μg/ml. The acetonitrile (Acetyl) 50% diluent for the peptide pool is presented as a no-peptide control. Each sample was measured in duplicate. The identifiers for the NHPs in each group are presented on the *x* axis.

cific T-cell responses on day 20 were observed only in those macaques challenged with live virus (Fig. 1E). Despite the clear differences in the responses between the three groups, attempts to detect replicating virus using quantitative PCR (qPCR) were unsuccessful for all animals and were thus suggestive of a technical fault rather than a lack of replicating virus.

In summary, only live pH1N1 was capable of eliciting clinical and cellular signs of infection. Live infection was characterized by elevated humoral and cellular responses, as well as a biphasic fever. Despite the small sample size ($n = 2$), previous vaccination with a CpG-adjuvanted vaccine containing both HA and NP antigens protected the challenged macaques from fever and potentiated postchallenge boosting of adaptive immune responses.

Transcriptional profiles of subclinical responses to mixed-particle aerosol pH1N1 influenza challenge. To investigate the subclinical responses to pH1N1 challenge, longitudinal blood samples were used to identify the timing and systems-level com-

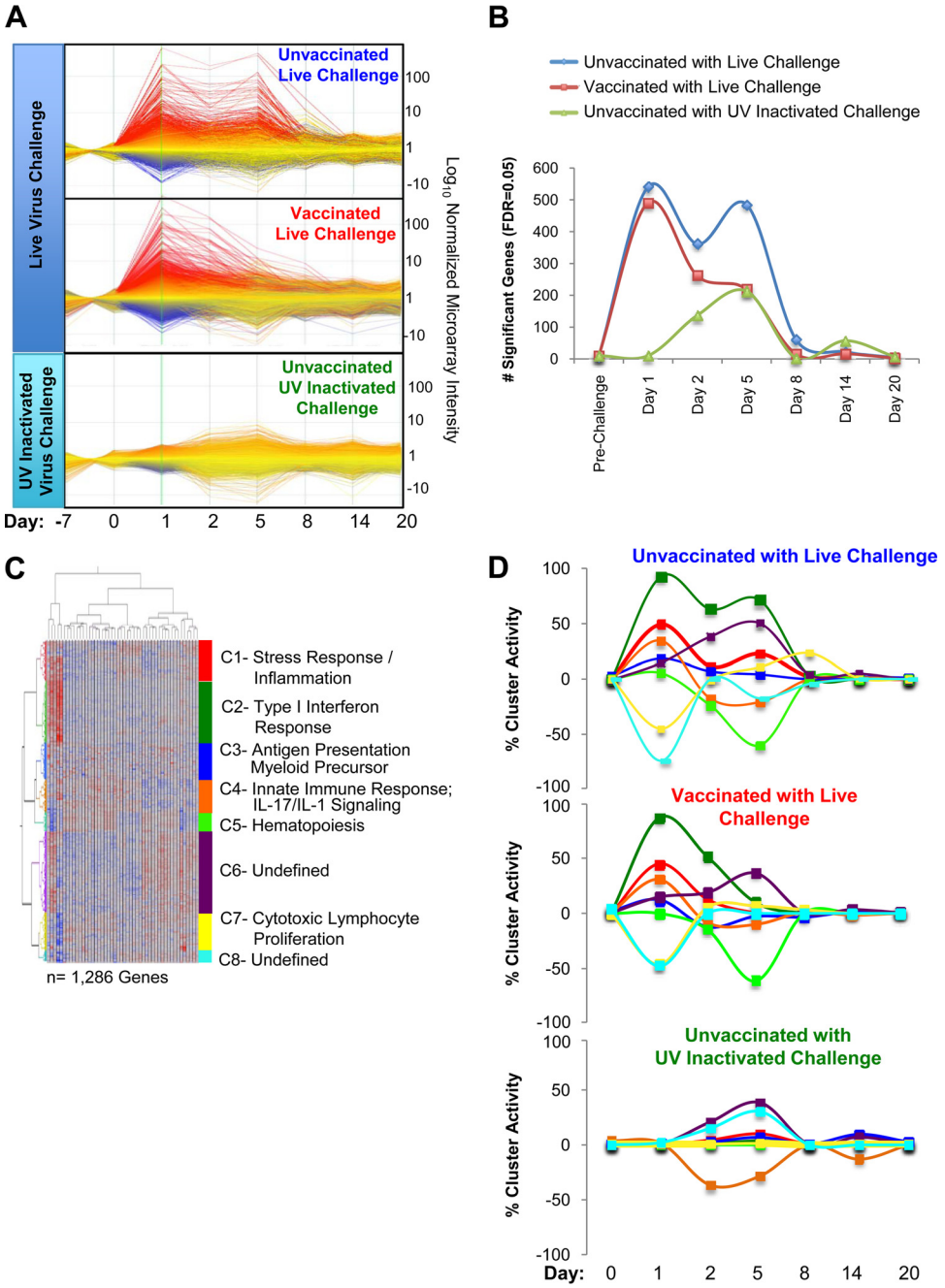

FIG 2 Whole blood transcriptional profiling reveals signatures associated with viral challenge. (A) Transcriptional activity of all expressed genes normalized to prechallenge baselines reveals global changes in transcriptional signatures that differentiate animals challenged with live pH1N1 virus and those challenged with UV-inactivated virus. Furthermore, animals previously vaccinated with anti-LOX-1-HA and anti-DCIR-NP fusion proteins exhibited reduced transcriptional perturbations, especially on day 5 after challenge with live virus. Linear mixed models were employed to identify genes with differential abundance for each of the three animal groups relative to their respective preinfection baselines. (B) Number of genes with significant changes in abundance were plotted at each time point for each group. (C) The genes in panel B were then hierarchically clustered, and k-means (k = 8) were used to group genes with similar expression profiles across the time points. GeneGo pathway analysis was employed to annotate each cluster (Table 1; also see Table S1 in the supplemental material). (D) Percent cluster activity was calculated at each time point by determining the ratio of significant genes to the total number of genes constituting the cluster. The sign of the LMMA statistical estimate was used to assign positive or negative cluster activity relative to the preinfection baseline. Color coding for each cluster matches that presented in the heat map in panel C.

positions of the immune responses to the pH1N1 virus. After the transcriptional activity for each expressed gene was normalized to the average prechallenge baseline expression, a clear picture of the mRNA expression changes was visualized between the animals challenged with live virus and those challenged with UV-inactivated virus (Fig. 2A). This global visualization of transcriptional activity also revealed qualitative signature differences following a live-virus challenge of the previously vaccinated animals with pro-

tective immunity (given by HAI assay titer of >40) versus that with naive animals (Fig. 2A).

In order to characterize the signature differences between the three experimental groups, linear mixed-model analysis (LMMA) was employed. LMMA identified transcripts with variable abundance at any time point between the 3 experimental groups and the shared prechallenge baseline. This analysis accounted for repeated measurements from the same animal over time and unequal time point spacing. In total, 1,286 transcripts displayed significant differential expression in at least one comparison to the shared baseline (false-discovery rate [FDR], 0.05). By plotting the number of gene transcripts for each experimental group found to be significantly altered in abundance relative to that of the prechallenge baseline (Fig. 2B), we identified time points that exhibited differences in the transcriptional changes for each group. The animals challenged with UV-inactivated virus exhibited a single peak of weak transcriptional perturbation that was maximal on day 5 postchallenge. In contrast, both the unvaccinated and vaccinated groups challenged with live virus exhibited biphasic changes in their transcriptional activities relative to baseline. Maximal perturbations for the naive macaques exposed to live virus were observed on days 1 and 5 postchallenge. Notably, there were 267 more significant transcripts observed in the unvaccinated group than in the previously vaccinated group on day 5 postchallenge.

k-means (k = 8) clustering was used to group transcripts with similar expression patterns across experimental time points. Gene ontology and network enrichment analysis were employed to annotate these 8 clusters (Table 1 and Fig. 2C; also see Table S1 in the supplemental material). To assess the longitudinal activity of each of these clusters relative to the prechallenge baseline, an activity score was determined for each cluster at each time point postchallenge. Briefly, this activity score represents the percentage of all genes within each cluster that were differentially expressed at each time point using LMMA. The sign associated with the mean estimate of the LMMA for the significant genes within each cluster at each time point was used to assign increased or decreased activity for each cluster (Fig. 2D). This analysis revealed that challenge with live virus elicited increased activity in type I interferon responses (cluster C2), stress response/inflammation (C1), and innate immune responses (C4) on day 1 postinfection. These pathways remained quiescent in the animals challenged with UV-inactivated virus. The activity for cytotoxic lymphocyte proliferation (C7) decreased compared to the baseline activity in the animals challenged with live virus but not in animals challenged with inactivated virus. On day 5 postchallenge, the type I interferon response cluster (C2) exhibited strong activation in the unvaccinated animals, and this response was notably reduced in the previously vaccinated group. Also, on day 5, the hematopoiesis cluster (C5) exhibited decreased activity in the animals challenged with live virus but not those challenged with inactivated pH1N1. A direct LMMA comparison between the vaccinated and unvaccinated groups at each time point revealed specific genes from each cluster that were differentially expressed between the vaccinated and unvaccinated arms (see Fig. S2 in the supplemental material).

Type I interferon activity is associated with subclinical fever responses 5 days postchallenge. While the cluster activity quantifies the number of genes that are significant for each cluster per time point, it fails to account for the magnitude of difference for the variable genes. Therefore, the molecular distance to health metric (MDTH) (21) was employed to quantify the sum expression difference for each cluster at each time point. Using this metric, only the type I interferon cluster (C2; $P = 0.01$) and antigen presentation cluster (C3; $P = 0.03$) exhibited significant differences between the vaccinated and unvaccinated groups on day 5 postchallenge (see Fig. S3 in the supplemental material). Since only the type I interferon cluster was significantly activated in the live-virus challenge compared to in the inactivated-virus challenge, we focused on this activity. Tightly regulated type I interferon responses play a key role in host responses to viral infection (22). The animals challenged with UV-inactivated virus failed to increase interferon activity over the baseline levels at all time points postchallenge. In contrast, on day 1 postchallenge, both the vaccinated and unvaccinated groups challenged with live virus exhibited significantly elevated interferon responses compared to those at baseline ($P < 0.01$) and on day 1 of the animals challenged with the UV-inactivated virus. On day 5 postchallenge, the interferon response in the unvaccinated live-virus challenge group was significantly elevated compared to that in both groups vaccinated with the live virus ($P = 0.014$) and the UV-inactivated virus ($P = 0.008$). The difference in the interferon activities between the live-virus challenge arm and the UV-inactivated-virus arm was not significant at this time point (Fig. 3A). When the average number of fever hours observed for the live challenge arm on day 5 was plotted as a function of interferon transcriptional activity ($\log_{10}$ MDTH), an association became apparent ($R^2 = 0.67$) (Fig. 3B). This association between interferon activity and clinical signs is similar to what has been documented in the context of human influenza virus responses (23). Interferon transcriptional activity was not found to be correlated ($R^2 = 0.001$) with peak body temperature, thus suggesting that day 5 interferon activity is more closely associated with fever duration rather than fever intensity. Thus, despite the weak subclinical response to mixed-particle aerosol pH1N1 influenza challenge in the rhesus macaques, the transcriptional activity of the type I interferon responses was found to associate closely with elevated body temperatures on 5 to 6 days postchallenge.

Application of type I interferon profiling in a candidate vaccine challenge model under subclinical response conditions. To further explore the hypothesis that measuring whole blood interferon responses could be used as a surrogate metric for candidate vaccine efficacy in the context of rhesus pH1N1 challenge, we initiated a follow-up study with larger cohorts ($n = 4$) to assess two different prototype influenza vaccines administered with poly(ICLC) (Hiltonol). The two vaccines tested varied only in the influenza virus antigen used, HA or NP (see Materials and Methods for details). Each vaccine was administered once every 6 weeks, for a total of 3 vaccinations, followed by a 6-week rest period before challenge with live pH1N1. Two control groups were included in this experiment: a Fluzone (2009 to 2010) vaccine that was not matched for the Cal04 pH1N1 strain was used to assess any cross-protection not associated with HA, and the vaccine vehicle medium–poly(ICLC) was used to control for any protection afforded by the adjuvant alone. Blood samples were collected on days −7, 0, 1, 3, 6, 14, and 20 postchallenge.

In order to confirm the immune responses elicited with the prototype vaccines, we measured the HA- and NP-specific antibody titers (Fig. 4A and B) and HAI assay titers (Fig. 4C) prior to and on 20 days postchallenge. As expected, the prechallenge titers for the anti-HA antibodies and the HAI assay were elevated only in

TABLE 1 Summary of GeneGo pathway analyses identifies networks enriched in each cluster[a]

	Enrichment by GO Processes	Total Genes	Genes In Data	p-value	FDR
Cluster 1: Stress Response / Inflammation (n=158)	cellular response to zinc ion	17	4	4.07E-06	2.16E-03
	cellular response to cadmium ion	17	4	4.07E-06	2.16E-03
	apoptotic process	1325	19	1.11E-05	3.23E-03
	negative regulation of growth	279	4	1.22E-05	3.23E-03
	plasma lipoprotein particle oxidation	2	2	4.34E-05	6.57E-03
	response to muscle inactivity	9	2	4.34E-05	6.57E-03
	lipid oxidation	82	2	4.34E-05	6.57E-03
	inflammatory response	593	12	6.09E-05	8.07E-03
	response to lithium ion	60	4	8.16E-05	9.61E-03
	positive regulation of adaptive immune response	128	3	9.76E-05	1.03E-02
Cluster 2: Type I Interferon Response (n=246)	defense response to virus	197	38	1.95E-37	2.95E-34
	type I interferon-mediated signaling pathway	87	24	5.96E-28	4.51E-25
	response to virus	322	25	1.88E-21	9.48E-19
	cytokine-mediated signaling pathway	439	32	2.73E-21	1.03E-18
	negative regulation of viral genome replication	46	14	2.93E-18	8.87E-16
	innate immune response	983	40	1.67E-16	4.21E-14
	immune response	1505	28	2.10E-12	4.53E-10
	interferon-gamma-mediated signaling pathway	94	13	1.58E-11	2.98E-09
	modulation by virus of host morphology or physiology	524	26	2.36E-11	3.97E-09
	defense response to Gram-positive bacterium	66	9	2.58E-08	3.90E-06
Cluster 3: Antigen presentation / Myeloid Precursor (n=146)	antigen processing and presentation of peptide antigen via MHC class I	157	9	1.36E-07	5.74E-05
	antigen processing and presentation of exogenous peptide antigen via MHC class I, TAP-independent	24	5	1.68E-07	5.74E-05
	immune response	1505	15	2.13E-07	5.74E-05
	positive regulation of cell proliferation in bone marrow	6	3	1.54E-06	3.12E-04
	antigen processing and presentation of exogenous peptide antigen via MHC class I, TAP-dependent	111	7	2.45E-06	3.95E-04
	antigen processing and presentation of exogenous peptide antigen via MHC class I	118	7	3.68E-06	4.95E-04
	type I interferon-mediated signaling pathway	87	6	7.88E-06	9.09E-04
	positive regulation of T cell mediated cytotoxicity	56	5	1.10E-05	1.11E-03
	interferon-gamma-mediated signaling pathway	94	6	1.23E-05	1.11E-03
	negative regulation of apoptotic process in bone marrow	3	2	2.92E-05	1.72E-03
Cluster 4: Innate Immune Response; IL-17/IL-1 Signaling (n=130)	positive regulation of transcription from RNA polymerase II promoter	1023	22	2.46E-08	2.26E-05
	immune response	1505	16	4.31E-08	2.26E-05
	negative regulation of apoptotic process	1022	18	6.08E-07	2.12E-04
	lipopolysaccharide-mediated signaling pathway	41	5	3.01E-06	7.88E-04
	positive regulation of transcription, DNA-dependent	1383	16	3.78E-06	7.92E-04
	apoptotic process	1325	17	1.28E-05	1.81E-03
	negative regulation of cell proliferation	802	13	1.60E-05	1.81E-03
	toll-like receptor signaling pathway	159	7	1.61E-05	1.81E-03
	toll-like receptor TLR6:TLR2 signaling pathway	98	6	1.73E-05	1.81E-03
	toll-like receptor TLR1:TLR2 signaling pathway	98	6	1.73E-05	1.81E-03
Cluster 5: Hematopoiesis (n=75)	oxygen transport	20	4	5.08E-07	2.65E-04
	fatty acid metabolic process	359	7	3.42E-06	8.93E-04
	response to lead ion	35	4	5.29E-06	9.20E-04
	apoptotic process in bone marrow	2	2	1.08E-05	1.41E-03
	positive regulation of plasma membrane long-chain fatty acid transport	3	2	3.22E-05	2.74E-03
	suppression by virus of host apoptotic process	3	2	3.22E-05	2.74E-03
	cell cycle arrest	194	6	3.67E-05	2.74E-03
	heme biosynthetic process	24	3	5.09E-05	2.80E-03
	protein heterooligomerization	160	5	5.22E-05	2.80E-03
	response to cycloheximide	7	2	6.43E-05	2.80E-03
Cluster 6: Undefined (n=324)	regulation of vasodilation	64	10	6.77E-13	1.38E-09
	G-protein coupled purinergic nucleotide receptor signaling pathway	18	7	2.75E-09	2.79E-06
	positive regulation of vasodilation	43	9	6.83E-09	4.62E-06
	regulation of systemic arterial blood pressure by norepinephrine-epinephrine	17	4	3.78E-08	1.38E-05
	positive regulation of the force of heart contraction by epinephrine	4	4	3.78E-08	1.38E-05
	inflammatory response	593	24	4.43E-08	1.38E-05
	regulation of calcium ion transport	221	9	4.75E-08	1.38E-05
	negative regulation of ossification	48	7	1.94E-07	4.00E-05
	microglial cell activation involved in immune response	11	5	2.25E-07	4.00E-05
	negative regulation of urine volume	11	5	2.25E-07	4.00E-05
Cluster 7: Cytotoxic Lymphocyte Proliferation (n=149)	phosphatidylinositol-mediated signaling	178	11	1.33E-08	1.79E-05
	cell surface receptor signaling pathway	3985	14	3.40E-08	2.28E-05
	positive regulation of phosphoprotein phosphatase activity	14	4	1.32E-06	5.92E-04
	mitotic cell cycle	852	14	3.21E-06	8.90E-04
	embryonic cleavage	16	4	3.32E-06	8.90E-04
	T cell activation	269	6	5.34E-06	1.19E-03
	transmembrane receptor protein tyrosine kinase signaling pathway	705	7	9.98E-06	1.70E-03
	mast cell chemotaxis	7	3	1.01E-05	1.70E-03
	Wnt receptor signaling pathway involved in somitogenesis	9	3	2.41E-05	2.31E-03
	platelet aggregation	26	4	2.59E-05	2.31E-03
Cluster 8: Undefined (n=45)	positive regulation of G-protein coupled receptor protein signaling pathway	28	3	9.77E-06	2.23E-03
	cardiac muscle cell apoptotic process	16	3	9.77E-06	2.23E-03
	regulation of autophagy	85	3	1.68E-05	2.56E-03
	positive regulation of epidermal growth factor receptor signaling pathway	36	3	2.30E-05	2.62E-03
	oocyte maturation	24	3	3.48E-05	3.17E-03
	activation of MAPK activity	190	5	4.31E-05	3.28E-03
	regulation of protein processing	62	2	6.93E-05	4.52E-03
	mitotic metaphase	6	2	1.04E-04	5.92E-03
	nucleosome positioning	7	2	1.45E-04	7.35E-03
	cellular response to carbohydrate stimulus	103	2	1.93E-04	8.81E-03

[a] For each cluster, the top 10 pathway maps, process networks, and gene ontology (GO) processes were identified. The size of each gene list is displayed under the total, with those genes found in both the network and the mixed-model-derived cluster listed under network objects from active data. Based on an interpretation of significant pathways, each cluster is annotated where appropriate.

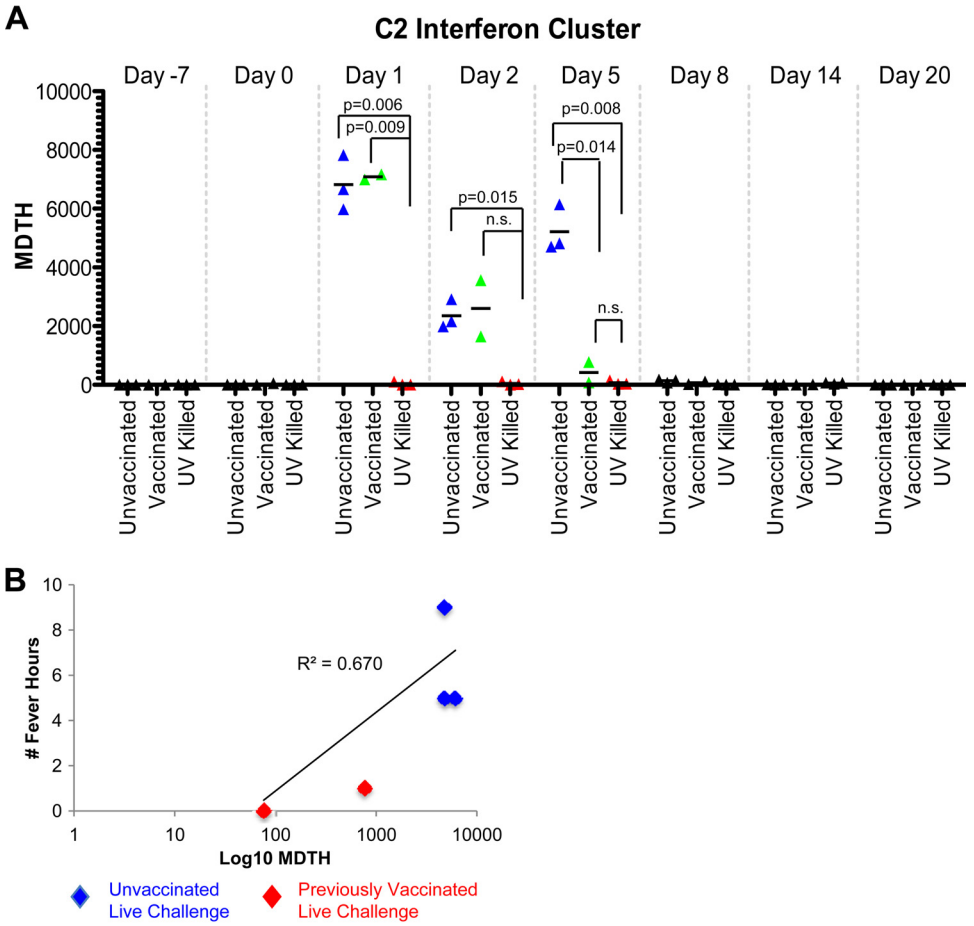

FIG 3 Vaccination reduces type I interferon 5 days after Cal04 challenge and is associated with a reduction in subclinical fever observations. (A) Activity of the interferon cluster relative to baseline (day −7 and day 0 average) for each animal was quantified using the molecular distance to health (MDTH) metric at each time point. An unpaired *t* test with Welch's correction was used to determine the significance of the observed differences. The actual *P* values are presented for relevant comparisons. n.s., nonsignificant. (B) Positive correlation between MDTH and the number of observed fever hours for each animal at day 5 postchallenge.

those macaques that received the anti-CD40-HA–poly(ICLC) vaccine, while the prechallenge titers for anti-NP antibodies were elevated only in those animals that received the anti-CD40-NP–poly(ICLC) vaccine. The HAI assay titers for the animals that received the NP vaccine were not determined. The animals in these control groups had low or undetectable titers against these antigens prior to challenge, and they also had undetectable HAI assay titers prior to challenge. On day 20 postchallenge, both control groups elicited low serum IgG levels for antibodies specific to both the HA and NP antigens. On day 20 postchallenge, both vaccine groups showed greatly increased serum IgG levels for antibodies specific to the indicated vaccine antigen component but not to the alternate antigen carried only by the live virus (Fig. 4C). The HAI assay titers were significantly elevated for all measured groups postchallenge ($P < 0.05$, paired *t* test). Together, these data suggest that the vaccines suppressed the development of neoantibodies specific to the nonvaccine components of the virus challenge compared to that of the control animals, which generally developed low but detectable antibodies specific to both the HA and NP virus antigens.

Next, we assessed the quantitative differences in the type I interferon activities between each postchallenge experimental arm (Fig. 4D). To accomplish this, we utilized the transcript list previously defined in cluster 2 of Fig. 1C to determine the MDTH of each group relative to a shared prechallenge baseline (all prechallenge samples on days −7 and 0 were used as the baseline). To account for repeated measurements and unequal time point spacing, LMMA was employed. On day 1 postchallenge, the interferon response of the anti-CD40-HA–poly(ICLC) group was found to be significantly less than either the Fluzone ($P = 0.03$) or the medium–poly(ICLC) control ($P = 0.04$) responses. However, there were no significant differences in the transcriptional activities between the vaccine arms at this time point. At day 3 postchallenge, the decreased interferon activity of the anti-CD40-HA–poly(ICLC) arm remained significant compared to the unmatched Fluzone response. Strikingly, by day 6, both vaccine groups exhibited very little type I interferon activity, while the medium–poly(ICLC) group response remained significantly elevated ($P = 0.01$). The Fluzone group exhibited an intermediate phenotype between the prototype vaccine groups and the medium–poly(ICLC) control groups. As was previously demonstrated, the interferon transcriptional activity resolved by day 14 postchallenge for all groups.

To determine if the postchallenge changes in interferon activity

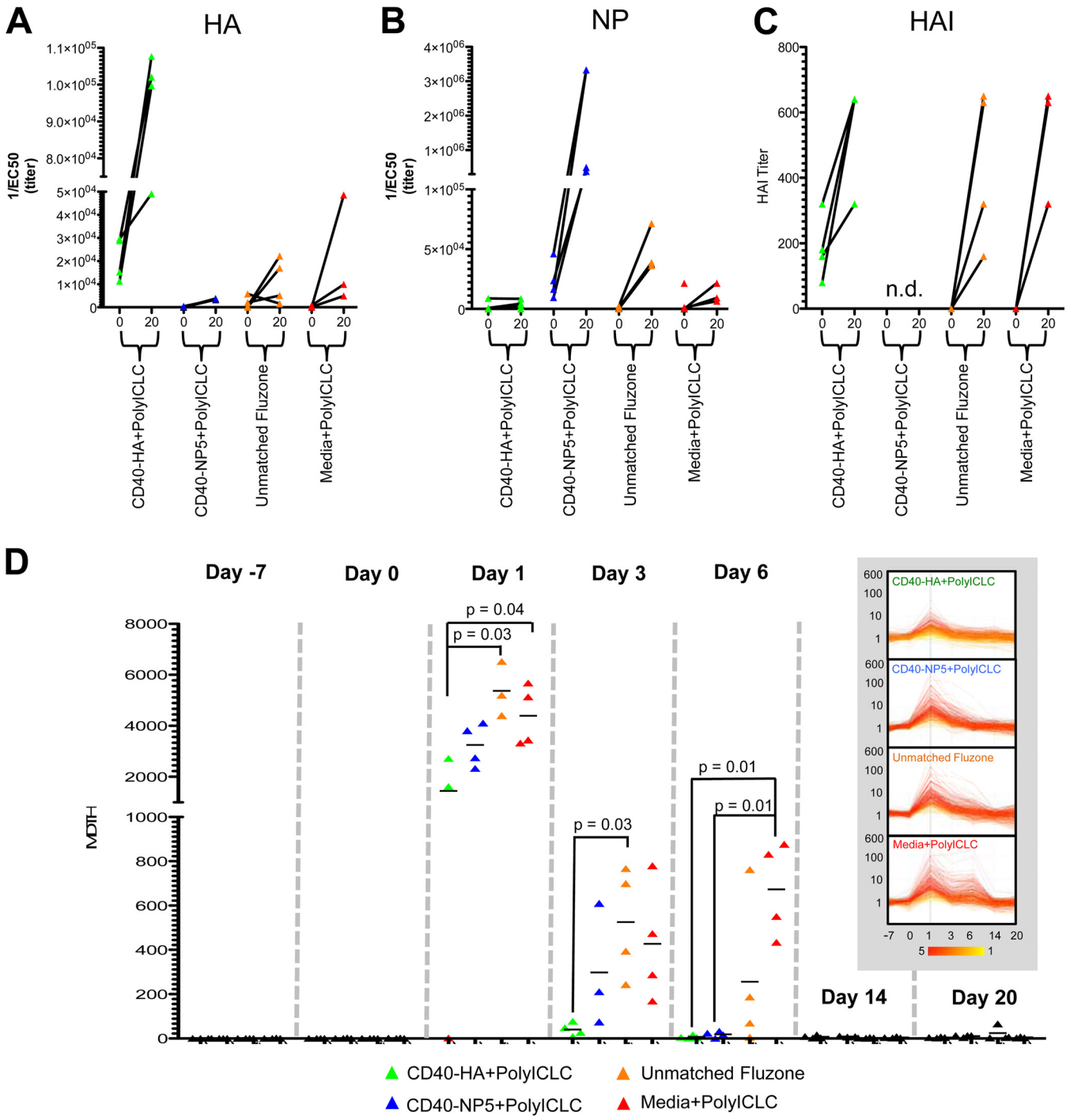

FIG 4 Reduced postchallenge interferon activity can be used as a surrogate marker to appraise protection imparted by candidate vaccines. Two different fusion protein vaccines [anti-CD40-HA–poly(ICLC) and anti-CD40-NP–poly(ICLC)], varying only in the type of flu antigen presented, were assessed as candidate vaccines. Four macaques per group received 3 subdermal injections of candidate vaccine plus poly(ICLC), poly(ICLC) alone, or unmatched Fluzone vaccine. The antibody titers to HA (A) and NP (B) were determined prior to challenge and on 20 days postinfection. (C) HAI neutralization titers were determined for all groups except for the NP vaccine group. (D) MDTH was calculated for those genes previously defined as type I interferon (C2) at days −7, 0, 1, 3, 6, 14, and 20 after challenge with pH1N1. Statistical comparisons between the groups at each time point were conducted using an unpaired *t* test with Welch's correction. The inset line graphs represent the global activity of C2 type I interferon normalized to the prechallenge baseline for each group.

reflected changes in the cellular composition of the blood or represented increased interferon activity by the existing circulating cells, complete blood counts (CBCs) were determined at each time point (see Fig. S4A to E in the supplemental material). Both the vaccinated and control cohorts exhibited significant lymphopenia ($0.0001 < P < 0.02$) and neutrophilia ($0.001 < P < 0.04$) on day 1 postchallenge. On day 6 postchallenge, only the Fluzone cohort exhibited an increase in circulating monocytes compared to base-

line. We further assessed the monocyte-to-lymphocyte ratio at each time point, since it has been reported to be a screening tool for influenza virus infection (24). All macaque groups exhibited a significant increase in the monocyte-to-lymphocyte ratio on day 1 postchallenge ($P < 0.0002$) but not on day 6. Since no significant changes in cellular composition were found to differentiate the previously vaccinated cohorts from the medium–poly(ICLC) group on day 6, the fever-associated interferon responses noted that time likely reflect changes in gene expression rather than changes in cellular frequency. The UV-inactivated virus also led to lymphopenia and neutrophilia (see Fig. S5A and B in the supplemental material). However, these responses were delayed in initiation (significant at day 2) and protracted in duration (significant from days 2 to 8) for the lymphocyte and neutrophil populations compared to the acute (day 1) responses following live virus challenge (see Fig. S4B and C and S5C to G in the supplemental material). In total, these CBC data suggest that the interferon responses, which were previously shown to vary on day 6 between the vaccinated and nonvaccinated groups (Fig. 4D), cannot be explained by changes in cell composition, suggesting that gene induction in the existing cell types accounts for the observed increases.

DISCUSSION

Historically, nonhuman primate models of human influenza virus infection have been selected for those with outwardly observable clinical signs that recapitulate the moderate-to-severe symptomatic responses observed in clinical human cases. By attaining a strong clinical phenotype, these can then be used to easily assess candidate vaccines as challenge models. The symptoms associated with such models are a function of the influenza virus strain, route of inoculation, dose of inoculation, and chosen primate species (25). In recent studies, high-dose administrations of pH1N1 virus to tracheal, nasal, ocular, and oral mucosal surfaces of rhesus macaques (*M. mulatta*) failed to elicit clinically observable symptoms despite detectable viral replication in the respiratory tract (6) and increased pulmonary inflammation measured by changes in effector lymphocyte populations, the secretion of inflammatory cytokines, and changes in bronchoalveolar lavage (BAL) gene expression (10).

Here, we attempted to establish a rhesus macaque model that recapitulated the clinical disease signs observed in humans. We hypothesized that deeper airway penetration of the virus, achieved through a naturally aspirated mixed-particle aerosol route of viral administration, would lead to increased signs of disease. However, our data indicate that rhesus macaques remain outwardly asymptomatic despite the administration of virus by mixed-particle aerosol administration. This occurred despite measurable signs of infection, including elevated body temperature, increased interferon activity, and changes in the frequency of circulating immune cells. These signs of active infection were either absent or significantly different in the naive animals receiving UV-inactivated virus.

Seasonal influenza challenge studies in human volunteers suggest that clinically asymptomatic responses to infection may be relatively common in the human population. In one human challenge study, only 21% (3 of 14) of the H3N2-challenged subjects and 11% (1 of 9) of the seasonal H1N1-challenged subjects developed fevers by day 7 postinfection, despite testing seronegative for the challenge strain (26). In a second study, only 9 of 17 volunteers infected with seasonal H3N2 developed mild-to-severe signs based on standardized symptom scoring, despite uniformly testing negative on the HAI assay at preinoculation screening and not previously being vaccinated (27). In both of these studies, the clinically asymptomatic volunteers exhibited subclinical signs of infection that were not outwardly expressed, including elevated body temperature, changes in gene expression, and changes in immune cell frequency, similar to the signs in the pH1N1-challenged rhesus macaques in this study.

The study by Huang et al. (27) went on to characterize the transcriptional signatures associated with both symptomatic and asymptomatic seasonal influenza virus infection using microarray-based profiling. These seasonal influenza virus signatures were then used to discriminate between pH1N1-infected and noninfected individuals in a clinical setting with 92% accuracy (23), thus suggesting that seasonal influenza virus signatures closely mirror those signatures resulting from pH1N1 infection in humans. This influenza virus signature was highly enriched in the antiviral interferon-related genes and was found to track closely with symptom scores over time. In our rhesus macaque model, we observed a similar association of interferon activity with a biphasic fever that peaked on days 1 and 5 to 6 postchallenge. This biphasic fever was similar to that previously observed in H5N1 infection in children (28) and in H5N1-infected rhesus macaques (29). The relationship between the interferon responses and fever has long been established (30), and fever is the major side effect of interferon-based therapies in humans (31). Thus, changes in IFN cluster transcript abundance in the blood might serve as a metric of subclinical host responses in this model of pH1N1 challenge.

The experimental vaccine combining anti-LOX-1-HA and anti-DCIR-NP with CpG-B coadministered 8 months previously resulted in a shorter duration of fever than that seen in the naive animals. This occurred despite the reduction in protective HAI assay titers to below the limit of detection at the time of challenge. This suggests that NP may provide a protective role that is more durable than that conferred by HA neutralization. The small sample size of this group limited our interpretation of these results and has prompted an expanded follow-up study.

This follow-up study used more primates per arm and added experimental control arms to further investigate the use of transcriptional immunomonitoring to measure host responses in this subclinical vaccine challenge model. The abilities of two candidate vaccines independently delivering HA and NP adjuvanted with poly(ICLC) to affect the type I interferon response following pH1N1 challenge were assessed and compared to those in primates treated with poly(ICLC) alone or vaccinated with a Fluzone split-virus vaccine. The Fluzone vaccine used was not matched for the challenge Cal04 pH1N1 strain and therefore was not expected to confer complete amelioration of the transcriptional responses. In this study, the only difference between the two candidate vaccines was the flu antigen presented by the fusion protein molecule. An anti-CD40-HA–poly(ICLC) vaccine presented the HA peptide sequence derived from pH1N1 strain Cal04, while an anti-CD40-NP5–poly(ICLC) vaccine presented NP antigen derived from the heterologous avian flu strain (H5N1). Despite being heterologous, NP5 and NP (Cal04) are 99.9% identical at the protein sequence level, highlighting the potential utility of this conserved flu antigen in a universal vaccine. Only in the macaques receiving the HA or NP5 vaccines were significant levels of serum anti-HA and anti-NP5 titers elicited. The HA-containing vaccine was able to reduce

both day-1 and day-6 interferon signatures, while the NP5-containing vaccine was only able to reduce the day-6 signature compared to that in the animals treated with medium–poly(ICLC). The difference in the postchallenge interferon responses between these two vaccines may reflect differences in the underlying immunologic mechanisms induced by each vaccine. Whereas the anti-CD40-HA–poly(ICLC) vaccine elicited protective neutralizing antibodies against pH1N1, as detected by the HAI assay, the anti-CD40-NP5–poly(ICLC) vaccine might act by eliciting cell-mediated responses that do not rely on viral neutralization to prevent infection (32). The trend toward lower interferon responses on day 1 postchallenge in the anti-CD40-HA–poly(ICLC) group might reflect reduced pH1N1 infection due to the presence of neutralizing antibodies. This contrasts with the anti-CD40-NP5–poly(ICLC)-vaccinated animals, in which there was no apparent reduction of the initial interferon responses on day 1 postchallenge; however, significantly reduced interferon-mediated responses on day 6 postchallenge were detected. The test vaccines presented here were pilot studies with small groups of monkeys, but they served to highlight the potential protective and/or ameliorative benefits of vaccination with both HA and NP proteins enhanced by DC-targeting approaches. The results from the extended studies are in preparation.

In conclusion, we have characterized a subclinical pH1N1 challenge model that recapitulates many phenotypes previously associated with pH1N1 infection. Because the primates in this model do not show outward clinical signs, we utilized telemetry and whole blood transcriptional profiling to identify pathways that might be used as surrogates of clinical illness. We were able to identify a biphasic fever response to challenge, which was associated with greatly increased type I interferon activity in the blood. By utilizing the transcriptional activity of this signature as a metric of host responses to challenge, we were able to assess two candidate vaccines for their ability to reduce the subclinical host responses to pH1N1 challenge. The ability to assess candidate vaccines in the absence of observable clinical signs and, in this case, detectable virus underscores the utility of our approach for meeting the unexpected challenges that might arise from newly emergent influenza virus strains. There is no guarantee that current influenza virus challenge models, including the symptomatic cynomolgus macaque model, will retain clinical signs of infection when infected with novel influenza virus strains. Therefore, having the ability to assess vaccine efficacy in subclinical settings may prove vital for future candidate vaccine assessment.

ACKNOWLEDGMENTS

We thank Andrew Lackner and Jacques Banchereau for supporting this study and Richard Cadagan for technical help with virus titrations and preparations. We also thank Robert Coffman for providing technical insight and access to the CpG adjuvant. We also thank Carson Harrod for review and editing of the manuscript.

Funding was provided by the National Institutes of Health grants 5U19AI057234, 5U19AI089987, 5U19AI057234S2, and 5U19AI057234S3. This work was also supported in part through NIH/OD grant OD-011104-51 (Tulane National Primate Research Center Base grant).

G.Z., S.O, J.A.S., M.J.K., and A.G.-S. contributed to the study design. M.J.K. and C.J.R. directed the viral challenge. K.R.-L. provided veterinary oversight. C.S. performed cell isolation and cell-based assays at the TNPRC. H.V.-O. performed telemetry and downstream telemetry analysis. R.A.A. and A.G.-S. provided viral stocks and assessed viral replication from BAL postchallenge. Y.X. performed the HAI assays. S.M.Z. performed ELISPOT and bead-based enzyme-linked immunosorbent assays (ELISAs). S.M.Z. and G.Z. made the targeting vaccine prototypes. A.M.S. provided the Hiltonol adjuvant and technical advice. J.A.S. and P.V. performed the microarray sample preparation. J.A.S. performed the microarray and statistical analyses. J.A.S., S.O., and G.Z. wrote the manuscript.

REFERENCES

1. **Palese P, Wang TT.** 2011. Why do influenza virus subtypes die out? A hypothesis. mBio **2**(5):e00150-11. http://dx.doi.org/10.1128/mBio.00150-11.
2. **Gerhard W.** 2001. The role of the antibody response in influenza virus infection. Curr. Top. Microbiol. Immunol. **260:**171–190.
3. **Murphy BR, Nelson DL, Wright PF, Tierney EL, Phelan MA, Chanock RM.** 1982. Secretory and systemic immunological response in children infected with live attenuated influenza A virus vaccines. Infect. Immun. **36:**1102–1108.
4. **Kreijtz JH, Fouchier RA, Rimmelzwaan GF.** 2011. Immune responses to influenza virus infection. Virus Res. **162:**19–30. http://dx.doi.org/10.1016/j.virusres.2011.09.022.
5. **Lamere MW, Moquin A, Lee FE, Misra RS, Blair PJ, Haynes L, Randall TD, Lund FE, Kaminski DA.** 2011. Regulation of antinucleoprotein IgG by systemic vaccination and its effect on influenza virus clearance. J. Virol. **85:**5027–5035. http://dx.doi.org/10.1128/JVI.00150-11.
6. **Boonnak K, Paskel M, Matsuoka Y, Vogel L, Subbarao K.** 2012. Evaluation of replication, immunogenicity and protective efficacy of a live attenuated cold-adapted pandemic H1N1 influenza virus vaccine in non-human primates. Vaccine **30:**5603–5610. http://dx.doi.org/10.1016/j.vaccine.2012.06.088.
7. **Herfst S, van den Brand JM, Schrauwen EJ, de Wit E, Munster VJ, van Amerongen G, Linster M, Zaaraoui F, van Ijcken WF, Rimmelzwaan GF, Osterhaus AD, Fouchier RA, Andeweg AC, Kuiken T.** 2010. Pandemic 2009 H1N1 influenza virus causes diffuse alveolar damage in cynomolgus macaques. Vet. Pathol. **47:**1040–1047. http://dx.doi.org/10.1177/0300985810374836.
8. **Itoh Y, Shinya K, Kiso M, Watanabe T, Sakoda Y, Hatta M, Muramoto Y, Tamura D, Sakai-Tagawa Y, Noda T, Sakabe S, Imai M, Hatta Y, Watanabe S, Li C, Yamada S, Fujii K, Murakami S, Imai H, Kakugawa S, Ito M, Takano R, Iwatsuki-Horimoto K, Shimojima M, Horimoto T, Goto H, Takahashi K, Makino A, Ishigaki H, Nakayama M, Okamatsu M, Takahashi K, Warshauer D, Shult PA, Saito R, Suzuki H, Furuta Y, Yamashita M, Mitamura K, Nakano K, Nakamura M, Brockman-Schneider R, Mitamura H, Yamazaki M, Sugaya N, Suresh M, Ozawa M, Neumann G, Gern J, Kida H, et al.** 2009. *In vitro* and *in vivo* characterization of new swine-origin H1N1 influenza viruses. Nature **460:**1021–1025. http://dx.doi.org/10.1038/nature08260.
9. **Safronetz D, Rockx B, Feldmann F, Belisle SE, Palermo RE, Brining D, Gardner D, Proll SC, Marzi A, Tsuda Y, Lacasse RA, Kercher L, York A, Korth MJ, Long D, Rosenke R, Shupert WL, Aranda CA, Mattoon JS, Kobasa D, Kobinger G, Li Y, Taubenberger JK, Richt JA, Parnell M, Ebihara H, Kawaoka Y, Katze MG, Feldmann H.** 2011. Pandemic swine-origin H1N1 influenza A virus isolates show heterogeneous virulence in macaques. J. Virol. **85:**1214–1223. http://dx.doi.org/10.1128/JVI.01848-10.
10. **Josset L, Engelmann F, Haberthur K, Kelly S, Park B, Kawoaka Y, García-Sastre A, Katze MG, Messaoudi I.** 2012. Increased viral loads and exacerbated innate host responses in aged macaques infected with the 2009 pandemic H1N1 influenza A virus. J. Virol. **86:**11115–11127. http://dx.doi.org/10.1128/JVI.01571-12.
11. **Go JT, Belisle SE, Tchitchek N, Tumpey TM, Ma W, Richt JA, Safronetz D, Feldmann H, Katze MG.** 2012. 2009 pandemic H1N1 influenza virus elicits similar clinical course but differential host transcriptional response in mouse, macaque, and swine infection models. BMC Genomics **13:**627. http://dx.doi.org/10.1186/1471-2164-13-627.
12. **Li D, Romain G, Flamar AL, Duluc D, Dullaers M, Li XH, Zurawski S, Bosquet N, Palucka AK, Le Grand R, O'Garra A, Zurawski G, Banchereau J, Oh S.** 2012. Targeting self- and foreign antigens to dendritic cells via DC-ASGPR generates IL-10-producing suppressive $CD4^+$ T cells. J. Exp. Med. **209:**109–121. http://dx.doi.org/10.1084/jem.20110399.
13. **Klechevsky E, Flamar AL, Cao Y, Blanck JP, Liu M, O'Bar A, Agouna-Deciat O, Klucar P, Thompson-Snipes L, Zurawski S, Reiter Y, Palucka AK, Zurawski G, Banchereau J.** 2010. Cross-priming $CD8^+$ T cells by targeting antigens to human dendritic cells through DCIR. Blood **116:**1685–1697. http://dx.doi.org/10.1182/blood-2010-01-264960.

14. **Roy CJ, Adams AP, Wang E, Leal G, Seymour RL, Sivasubramani SK, Mega W, Frolov I, Didier PJ, Weaver SC.** 2013. A chimeric Sindbis-based vaccine protects cynomolgus macaques against a lethal aerosol challenge of eastern equine encephalitis virus. Vaccine **31:**1464–1470. http://dx.doi.org/10.1016/j.vaccine.2013.01.014.
15. **Romain G, van Gulck E, Epaulard O, Oh S, Li D, Zurawski G, Zurawski S, Cosma A, Adam L, Chapon C, Todorova B, Banchereau J, Dereuddre-Bosquet N, Vanham G, Le Grand R, Martinon F.** 2012. CD34-derived dendritic cells transfected *ex vivo* with HIV-Gag mRNA induce polyfunctional T-cell responses in nonhuman primates. Eur. J. Immunol. **42:**2019–2030. http://dx.doi.org/10.1002/eji.201242478.
16. **Flamar AL, Zurawski S, Scholz F, Gayet I, Ni L, Li XH, Klechevsky E, Quinn J, Oh S, Kaplan DH, Banchereau J, Zurawski G.** 2012. Noncovalent assembly of anti-dendritic cell antibodies and antigens for evoking immune responses *in vitro* and *in vivo*. J. Immunol. **189:**2645–2655. http://dx.doi.org/10.4049/jimmunol.1102390.
17. **Flamar AL, Xue Y, Zurawski SM, Montes M, King B, Sloan L, Oh S, Banchereau J, Levy Y, Zurawski G.** 2013. Targeting concatenated HIV antigens to human CD40 expands a broad repertoire of multifunctional $CD4^+$ and $CD8^+$ T cells. AIDS **27:**2041–2051. http://dx.doi.org/10.1097/QAD.0b013e3283624305.
18. **Friedberg JW, Kim H, McCauley M, Hessel EM, Sims P, Fisher DC, Nadler LM, Coffman RL, Freedman AS.** 2005. Combination immunotherapy with a CpG oligonucleotide (1018 ISS) and rituximab in patients with non-Hodgkin lymphoma: increased interferon-alpha/beta-inducible gene expression, without significant toxicity. Blood **105:**489–495. http://dx.doi.org/10.1182/blood-2004-06-2156.
19. **Rosenfeld MR, Chamberlain MC, Grossman SA, Peereboom DM, Lesser GJ, Batchelor TT, Desideri S, Salazar AM, Ye X.** 2010. A multi-institution phase II study of poly-ICLC and radiotherapy with concurrent and adjuvant temozolomide in adults with newly diagnosed glioblastoma. Neuro Oncol. **12:**1071–1077. http://dx.doi.org/10.1093/neuonc/noq071.
20. **Wang S, Taaffe J, Parker C, Solorzano A, Cao H, García-Sastre A, Lu S.** 2006. Hemagglutinin (HA) proteins from H1 and H3 serotypes of influenza A viruses require different antigen designs for the induction of optimal protective antibody responses as studied by codon-optimized HA DNA vaccines. J. Virol. **80:**11628–11637. http://dx.doi.org/10.1128/JVI.01065-06.
21. **Pankla R, Buddhisa S, Berry M, Blankenship DM, Bancroft GJ, Banchereau J, Lertmemongkolchai G, Chaussabel D.** 2009. Genomic transcriptional profiling identifies a candidate blood biomarker signature for the diagnosis of septicemic melioidosis. Genome Biol. **10:**R127. http://dx.doi.org/10.1186/gb-2009-10-11-r127.
22. **Ivashkiv LB, Donlin LT.** 2013. Regulation of type I interferon responses. Nat. Rev. Immunol. **14:**36–49. http://dx.doi.org/10.1038/nri3581.
23. **Woods CW, McClain MT, Chen M, Zaas AK, Nicholson BP, Varkey J, Veldman T, Kingsmore SF, Huang Y, Lambkin-Williams R, Gilbert AG, Hero AO, III, Ramsburg E, Glickman S, Lucas JE, Carin L, Ginsburg GS.** 2013. A host transcriptional signature for presymptomatic detection of infection in humans exposed to influenza H1N1 or H3N2. PLoS One **8:**e52198. http://dx.doi.org/10.1371/journal.pone.0052198.
24. **Merekoulias G, Alexopoulos EC, Belezos T, Panagiotopoulou E, Jelastopulu DM.** 2010. Lymphocyte to monocyte ratio as a screening tool for influenza. PLoS Curr. **2:**RRN1154. http://dx.doi.org/10.1371/currents.RRN1154.
25. **O'Donnell CD, Subbarao K.** 2011. The contribution of animal models to the understanding of the host range and virulence of influenza A viruses. Microbes Infect. **13:**502–515. http://dx.doi.org/10.1016/j.micinf.2011.01.014.
26. **Wilkinson TM, Li CK, Chui CS, Huang AK, Perkins M, Liebner JC, Lambkin-Williams R, Gilbert A, Oxford J, Nicholas B, Staples KJ, Dong T, Douek DC, McMichael AJ, Xu XN.** 2012. Preexisting influenza-specific $CD4^+$ T cells correlate with disease protection against influenza challenge in humans. Nat. Med. **18:**274–280. http://dx.doi.org/10.1038/nm.2612.
27. **Huang Y, Zaas AK, Rao A, Dobigeon N, Woolf PJ, Veldman T, Øien NC, McClain MT, Varkey JB, Nicholson B, Carin L, Kingsmore S, Woods CW, Ginsburg GS, Hero AO, III.** 2011. Temporal dynamics of host molecular responses differentiate symptomatic and asymptomatic influenza A infection. PLoS Genet. **7:**e1002234. http://dx.doi.org/10.1371/journal.pgen.1002234.
28. **Hall CB, Douglas RG, Jr.** 1975. Nosocomial influenza infection as a cause of intercurrent fevers in infants. Pediatrics **55:**673–677.
29. **Shinya K, Gao Y, Cilloniz C, Suzuki Y, Fujie M, Deng G, Zhu Q, Fan S, Makino A, Muramoto Y, Fukuyama S, Tamura D, Noda T, Eisfeld AJ, Katze MG, Chen H, Kawaoka Y.** 2012. Integrated clinical, pathologic, virologic, and transcriptomic analysis of H5N1 influenza virus-induced viral pneumonia in the rhesus macaque. J. Virol. **86:**6055–6066. http://dx.doi.org/10.1128/JVI.00365-12.
30. **Dinarello CA, Bernheim HA, Duff GW, Le HV, Nagabhushan TL, Hamilton NC, Coceani F.** 1984. Mechanisms of fever induced by recombinant human interferon. J. Clin. Invest. **74:**906–913. http://dx.doi.org/10.1172/JCI111508.
31. **Ingimarsson S, Cantell K, Strander H.** 1979. Side effects of long-term treatment with human leukocyte interferon. J. Infect. Dis. **140:**560–563. http://dx.doi.org/10.1093/infdis/140.4.560.
32. **Hashem AM, Gravel C, Chen Z, Yi Y, Tocchi M, Jaentschke B, Fan X, Li C, Rosu-Myles M, Pereboev A, He R, Wang J, Li X.** 2014. CD40 ligand preferentially modulates immune response and enhances protection against influenza virus. J. Immunol. **193:**722–734. http://dx.doi.org/10.4049/jimmunol.1300093.